applied sciences

MDPI

Article

Arrangement of Live Human Cells through Acoustic Waves Generated by Piezoelectric Actuators for Tissue Engineering Applications

Marialaura Serzanti [1], Marco Baù [2], Marco Demori [2], Serena Calamaio [1], Manuela Cominelli [3], Pietro Luigi Poliani [3], Patrizia Dell'Era [1,*], Marco Ferrari [2,*] and Vittorio Ferrari [2]

1 Cellular Fate Reprogramming Unit, Department of Molecular and Translational Medicine, University of Brescia, 25121 Brescia, Italy; m.serzanti@unibs.it (M.S.); s.calamaio@unibs.it (S.C.)
2 Department of Information Engineering, University of Brescia, 25121 Brescia, Italy; marco.bau@unibs.it (M.B.); marco.demori@unibs.it (M.D.); vittorio.ferrari@unibs.it (V.F.)
3 Pathology Unit, Department of Molecular and Translational Medicine, University of Brescia, 25121 Brescia, Italy; elemanu2003@libero.it (M.C.); luigi.poliani@unibs.it (P.L.P.)
* Correspondence: patrizia.dellera@unibs.it (P.D.); marco.ferrari@unibs.it (M.F.)

Received: 29 March 2020; Accepted: 14 May 2020; Published: 18 May 2020

Featured Application: The proposed device and method can promote the arrangement of cells in defined geometries through acoustic flexural plate waves for organized engineered tissues.

Abstract: In this paper, the possibility to steer and confine live human cells by means of acoustic waves, such as flexural plate waves (FPWs), generated by piezoelectric actuators applied to non-piezoelectric substrates, has been explored. A device with two lead zirconate titanate (PZT) actuators with an interdigital transducer (IDT) screen-printed on an alumina (Al_2O_3) substrate has been fabricated and tested. The experimental results show that, by exciting the actuators at their resonant frequencies, FPW modes are generated in the substrate. By exploiting the device, arrangements of cells on lines at frequency-dependent distances have been obtained. To maintain the alignment after switching off the actuator, cells were entrapped in a fibrin clot that was cultured for several days, enabling the formation of cellular patterns.

Keywords: acoustic waves; piezoelectric actuators; flexural plate waves (FPWs); in-liquid cell steering and confining; cell manipulation; tissue engineering applications; fibrin gel; myoblasts; endothelial cells

1. Introduction

So-called "tissue engineering science" refers to the practice of combining cells, biomaterials, and suitable biochemical and physicochemical factors to assemble a biological functional tissue. Tissue engineering science is emerging as a promising technique to build functional constructs that restore, maintain, or improve damaged tissues [1].

The physical and structural properties of the tissue, along with biological and biochemical environments, play key roles in achieving cell differentiation, maturation, and organogenesis [2]. Hence, the field of tissue engineering relies on the search for a three-dimensional (3D) scaffold representing a template for tissue formation that can be used in vivo, where it can act as a guidance for cellular regeneration, or can be seeded in vitro with cells and growth factors or subjected to biophysical/mechanical/chemical stimuli that promote tissue growth [3].

A crucial step in building a 3D tissue lies in its thickness, because the exceeding of a certain size (from 100 to 200 μm) prevents the oxygen, nutrients, and metabolic exchange among cell layers, irreparably leading to tissue necrosis [4]. To overcome this issue, current strategies rely on in vitro settings that increase the diffusion/perfusion of the tissue, such as a dynamic culture, while in vivo the colonization of the tissue by host vessels after grafting is promoted. Nevertheless, as happens in natural tissues, the fabrication of a network of microvessels that can be integrated with the host vasculature, could increase the survival of cells more sensitive to reduction of supply of nutrients and oxygen [5].

In recent research activities, 3D bioprinting, wherein both the layer-by-layer precise positioning of biological materials, biochemicals, and living cells, and the spatial control of the placement of functional components has been adopted, allowed for the fabrication of 3D structures exploiting bio-mimicry, autonomous self-assembly, and mini-tissue building blocks [6]. These goals can be pursued with the help of different deposition and shaping techniques, such as inkjet, microextrusion, and laser assisted printing, although these innovative technologies require expensive instrumentation. Bioprinters and bioplotters typically adopt piezoelectric or pneumatic devices for depositing cells, even dispersed into a proper liquid solution [7], and have the benefit of the flexibility of customizable patterning design, but have several drawbacks, such as the relatively large amount of time necessary to correctly achieve the spatial location of cells within the hydrogel, and limitations with respect to the density and viscosity of the liquid solution in which the cells need to be dispersed [8]. The main challenge remains the reproduction of the complex microarchitecture of extracellular matrix components with sufficient resolution, in which multiple cell types interact and exert their biological functions [9].

As an alternative, several strategies for cell trapping have been proposed and exploited in the literature. The most straightforward is hydrodynamic cell trapping, where a (series of) microchannel(s) of sufficiently small size in order to trap cells by suction is fabricated within microsystems [10]. Microbioreactors allowing direct-perfusion of culture medium through tissue-engineered constructs may overcome diffusion limitations associated with static culturing and may provide flow-mediated mechanical stimuli. The hydrodynamic stress imposed on cells within scaffolds is directly dependent on scaffold microstructure and on bioreactor configuration [11].

Microfluidic systems based on acoustic waves generated through the piezoelectric effect have recently received a great deal of attention in biological and medical fields for mixing, sorting, separation, counting, and positioning of particles and cells, mostly relying on the nodes and antinodes generated by standing waves [12]. Surface acoustic wave (SAW), bulk acoustic wave (BAW), and FPW (flexural plate wave) acoustic modes can be generated and detected by piezoelectric actuators driven at suitable frequencies to obtain wavelengths in the order of up to 100 μm [13,14]. The forces generated by the interaction between acoustic waves and fluids can be used to actuate fluids and suspended particles, such as cells, at a small scale with micrometric resolution. Additionally, piezoelectric devices have the inherent advantage of allowing contactless operation between the transducer and the electronics [15].

Custom-built microfluidic perfusion bioreactors with integrated ultrasound standing wave traps have been proposed for cartilage tissue engineering [16]. In such devices, acoustic waves and continuous perfusion of the culture medium at a low-shear flow rate promote scaffold-free generation of 3D agglomerates of human articular chondrocytes and enhance cartilage formation by cells of the agglomerates via improved mechanical stimulation and mass transfer rates. A versatile SAW technique has been proposed to control the distance between two isolated cells, to drive the clustering of single cells in defined geometries, by maintaining them in suspension, and transferring them to their adherent state [17]. The typical configuration of the microfluidic devices used for fluid and particle manipulations exploiting SAWs or FPWs requires piezoelectric substrates with interdigital transducers (IDTs) to realize the actuators [18–22].

In this study, the use of screen-printed piezoelectric films for the generation of the FPWs on alumina substrate was explored to assemble 1D cellular structures. The aim was to demonstrate that arrangements of living human cells can be advantageously obtained by acoustic waves with

actuators on generic non-piezoelectric substrates, thereby including transparent substrates typically adopted for the fabrication of microfluidic devices. This is advantageous compared to similar devices, both those based on FPWs and those based on SAWs, because non-piezoelectric substrates ease the patterning of IDTs in different positions without the need to consider the crystallographic orientations. Thus, by adding one or more pairs of IDTs, in principle it could be possible to obtain 2D-cellular structures. From a biological point of view, the use of the proposed device enables the formation of ordered cellular structures that can be merged into an engineered tissue.

2. Design and Fabrication of the Device

A sketch of the device developed to steer and confine cells dispersed in liquid is shown in Figure 1a. The device exploits two piezoelectric actuators placed diametrically opposed on the bottom of a 25 mm in diameter circular alumina (Al_2O_3) substrate to generate standing acoustic waves, as schematically represented in Figure 1b. The distance between pressure nodes, in which the cells are expected to be confined, corresponds to half the wavelength of the generated acoustic waves.

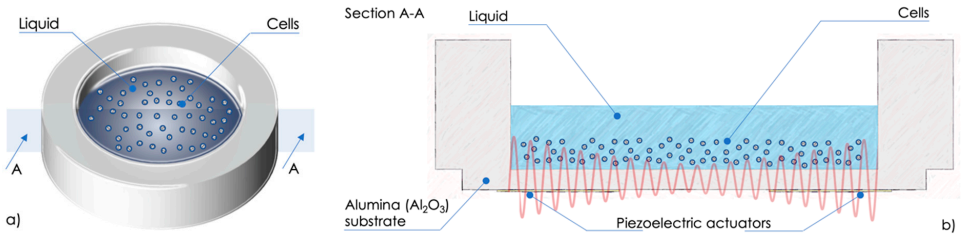

Figure 1. Sketch (**a**) and cross-section A-A (**b**) of the device developed to steer and confine cells dispersed in liquid.

The two piezoelectric actuators have been fabricated by the screen-printing technique [23]. Figure 2a,b show a section and a bottom view of the device, respectively, while Figure 2c shows an enlarged view of a cross-section of the piezoelectric actuator.

The fabrication process of the actuators starts with the screen-printing deposition of a palladium-silver (PdAg) ink to create the bottom 6 mm × 6 mm electrode (connected to pad C) on a 635-µm-thick alumina substrate, as shown in Figure 2d. Then drying at 150 °C and firing at 850 °C processes are applied to finalize the bottom electrode. A lead zirconate titanate (PZT) 8 mm × 8 mm layer is realized on top of the bottom electrode with multiple screen-printing depositions to obtain the final thickness of about 100 µm, as shown in Figure 2e. Drying at 150 °C and firing at 950 °C peak temperature are carried out to each PZT deposition. Finally, an IDT composed of two interleaved comb-shaped arrays of metallic electrodes (connected to pads A and B) is realized on top of the PZT layer by a deposition of PdAg ink, as shown in Figure 2f. Final drying and firing processes are applied to the IDT electrodes, as for the bottom electrode. The IDT has finger width and spacing of 350 µm, as shown in Figure 2c,f.

The PZT layer has been poled at 4 MV/m along the thickness by applying a DC voltage between the two armatures formed by A and B electrically shorted and C, respectively. Thus, a sinusoidal excitation voltage applied between A and B (with C floating), or between A and B electrically shorted and C, generates sinusoidal deformation along the PZT-layer thickness by exploiting mainly the d_{33} mode in both cases, since the thickness of the PZT layer is thinner than the spacing between two adjacent IDT fingers.

Compared to similar devices [12–14], a larger volume of liquid can be used. This is granted by the thickness of the screen-printed PZT film in the order of hundreds of micrometers and typically higher piezoelectric coefficients compared to piezoelectric crystals, thereby providing comparatively higher effectiveness of the actuators. The screen-printed deposition of PZT can be applied to other non-piezoelectric substrates, such as high-temperature glasses, which could grant optical transparency to the device.

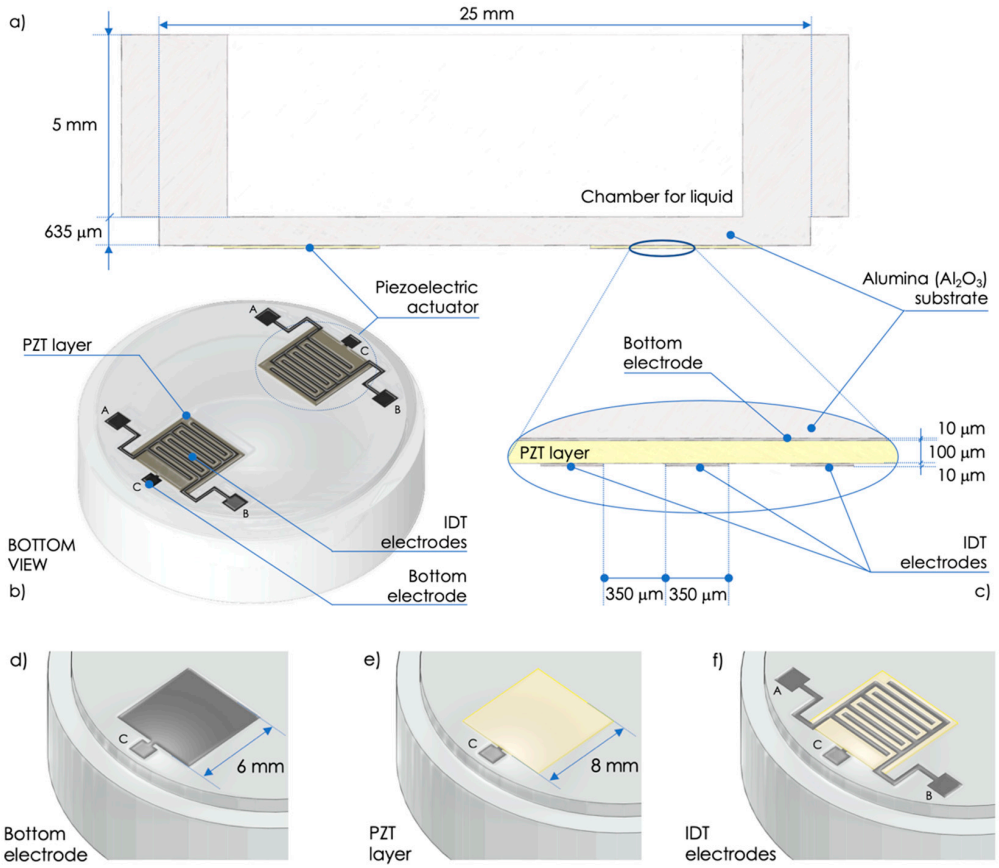

Figure 2. Section (**a**) and bottom view (**b**) of the device. Enlarged view of a cross-section of the piezoelectric actuator (**c**). Fabrication process: deposition of the bottom electrode (**d**), lead zirconate titanate (PZT) layer (**e**), and interdigital transducer (IDT) electrodes (**f**).

Figure 3a,b show top-view and bottom-view pictures of the fabricated device fixed to a printed circuit board (PCB) for electrical connections, respectively. The device can be used by filling the 5-mm-high chamber with liquid in which the cells are dispersed and where the generation of standing acoustic FPWs is expected.

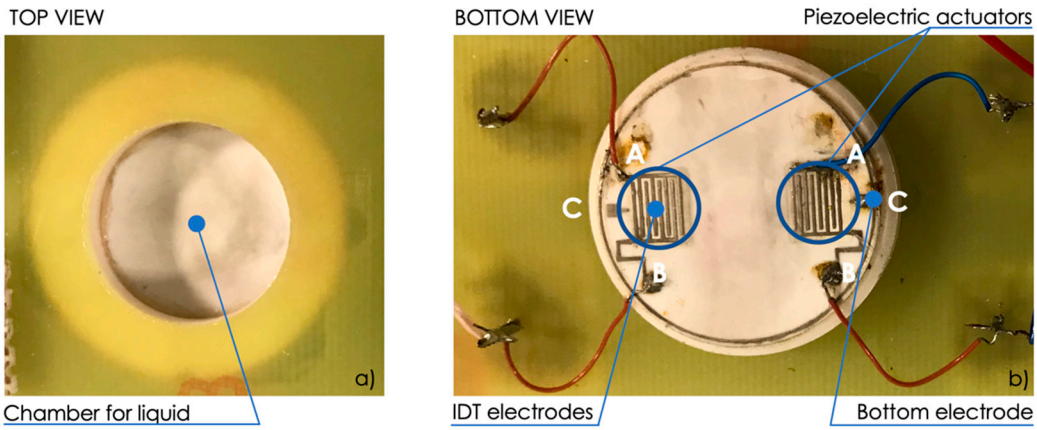

Figure 3. Top-view (**a**) and bottom-view (**b**) pictures of the fabricated device fixed to a printed circuit board (PCB).

3. Materials and Methods

3.1. Reagents

Bovine fibrinogen 90% clottable and bovine thrombin, high purity grade, were purchased from MP Biomedicals. Neutral Red was purchased from AMRESCO. 4',6-Diamidine-2'-phenylindole dihydrochloride (DAPI) was purchased by Sigma.

3.2. Cell Culture

L6 rat myoblasts and human foreskin fibroblasts (HFF; provided by American Type Culture Collection, catalogue #CRL-2429) were maintained in Dulbecco's modified Eagle's medium (Life Technologies) supplemented with 15% (*v*/*v*) fetal bovine serum (Life Technologies), 1% (*v*/*v*) non-essential amino acids (Life Technologies), and 1% (*v*/*v*) penicillin/streptomycin (Life Technologies). Cells were trypsinized every 3 or 4 days and split 1:4, with medium changes every other day.

Human umbilical vein endothelial cells (HUVECs) were isolated from human umbilical cords, used at early (I–IV) passages, and grown on plastic surface coated with 0.1% (*w*/*v*) porcine gelatin in Clonetics® EGM™-2 medium (Lonza). Cells were trypsinized every 3 or 4 days and split 1:4, with medium changes every other day. HUVECs were obtained from pregnant women, in accordance with the protocol approved by the Ethics Committee of Brescia (protocol number 1842).

Human adipose-derived mesenchymal stem cells (hMSCs) were obtained from a previous study described in [24]. Cells were maintained in Iscove's modified Dulbecco's medium containing 5% (*v*/*v*) human platelet lysate (STEMCELL™ Technologies) and 2U/mL heparin (Sigma). Cells were trypsinized every 3 or 4 days, and subcultures were seeded at 5000 cells/cm^2 with medium changes every other day. Cells from a single donor were used up to passage 6.

For human samples, written informed consents were obtained from patients in accordance with the Declaration of Helsinki.

3.3. Cell Viability Tests

Cells were counted using TC20™ Automated Cell Counter (BIO-RAD) that exploits auto-focus technology and sophisticated cell counting algorithms to produce accurate cell counts in less than 30 s. Viability tests were performed by adding to cell suspension one volume of the Trypan Blue Dye, 0.4% (*w*/*v*) solution. The presence of the blue dye inside a cell leads the machine to consider it as dead cells, thereby enabling the calculation of cell viability. Results are then reported as a percentage of total cell number.

3.4. Cell Staining

For the Neutral Red staining, cells were detached, resuspended in phosphate buffer saline (PBS) containing 40 µg/mL Neutral Red, incubated for 20 min, and directly used for the experiment.

For the nuclear fluorescent staining, DAPI was diluted to a final concentration of 1 µg/mL and incubated for 5 min. Cells were then washed twice with PBS before imaging.

3.5. Cell Alignment

Cells were detached and counted. A total of 10^6 cells were resuspended in 0.5 mL ice-cold culture medium. Cell suspension was transferred to the chamber for the actuation and the following microscopical observation.

To embed the cells in a clot, 10 mg/mL fibrinogen was added to cell culture medium without serum. Just before the transfer to the chamber for actuation, 2 µL of thrombin solution (200 U/mL in 0.9% NaCl) was added to the cell suspension. Actuation was performed for 5 min at the indicated frequency in order to allow for a complete clot polymerization.

The clot was transferred to a cell culture multiwell plate, covered with cell medium, and observed in the following days.

3.6. Clot Histology and Antibody Staining

Fibrin clot was fixed in 4% (*w*/*v*) paraformaldehyde (Bio-Optica) and processed for inclusion. The 2-µm-thick representative sections from paraffin embedded blocks were de-waxed and rehydrated. Endogenous peroxidase activity was blocked with 0.3% (*v*/*v*) H_2O_2 (Sigma Aldrich) in methanol for 20 min. Antigen retrieval was performed using a microwave oven in 1.0 mM EDTA (Carlo Erba) buffer (pH 8.0).

Sections were then washed in tris-buffered saline (TBS, Carlo Erba) (pH 7.4) and incubated for one hour in the specific primary antibody diluted in TBS 1% (*w*/*v*) bovine serum albumin (BSA) (CD31 (clone PECAM-1) Novocastra TM 1:50).

The signal was revealed using the DAKO Envision+System-HRP Labelled Polymer Anti-Mouse, followed by diaminobenzydine (DAB) as chromogen and hematoxylin as counterstain.

4. Results and Discussion

4.1. Electrical Characterization of the Device

The IDT actuators have been characterized experimentally in order to extract the frequencies at which the maximum FPW generation effectiveness is expected. Figure 4a,b show the admittances $Y_{A\text{-}B}$ and $Y_{AB\text{-}C}$ measured between A and B while C was floating, and between A and B electrically shorted and C, respectively.

The resonant frequencies of the two configurations, i.e., the frequencies where the conductance reaches a maximum [25,26], are at about 6.7 and 8.0 MHz for $Y_{A\text{-}B}$, and at about 6.0 and 7.2 MHz for $Y_{AB\text{-}C}$. These frequencies are expected to correspond to the propagation of FPW modes in the substrate [27,28].

A tailored electronic interface has been developed to drive the actuators. Figure 5 shows a block diagram of the interface. The excitation signals were generated by a programmable direct digital synthesizer (DDS, AD9959) that allowed us to excite the actuators with two independent channels and provided the possibility of setting both the common excitation frequency and the phase difference between the channels.

Dedicated power amplifiers (ADA4870) have been adopted as the output stage to properly drive the actuators. The electronic interface excites the actuators with a sinusoidal signal with peak-to-peak amplitude and frequency of up to 20 V and 15 MHz, respectively.

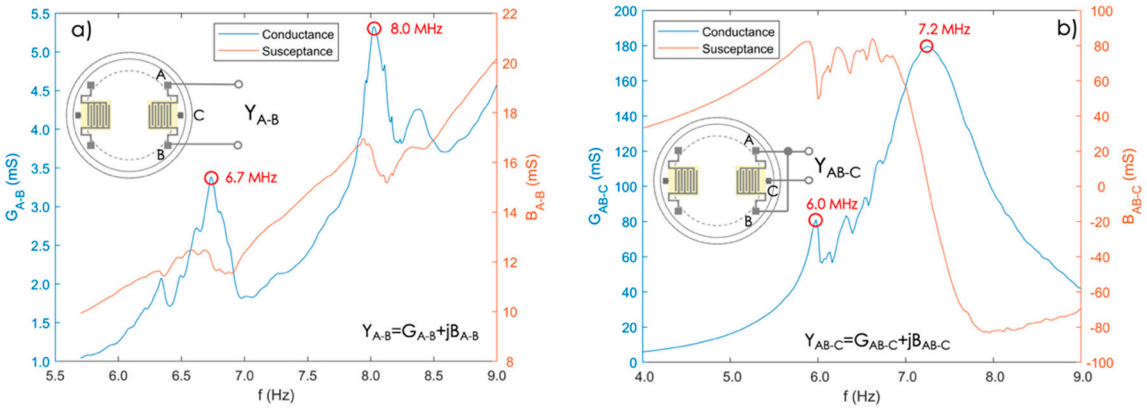

Figure 4. Measured admittance $Y_{A\text{-}B}$ (**a**) and $Y_{AB\text{-}C}$ (**b**) as functions of frequency. The plots show resonances at frequencies around 6.7 and 8.0 MHz (**a**) and around 6.0 and 7.2 MHz (**b**).

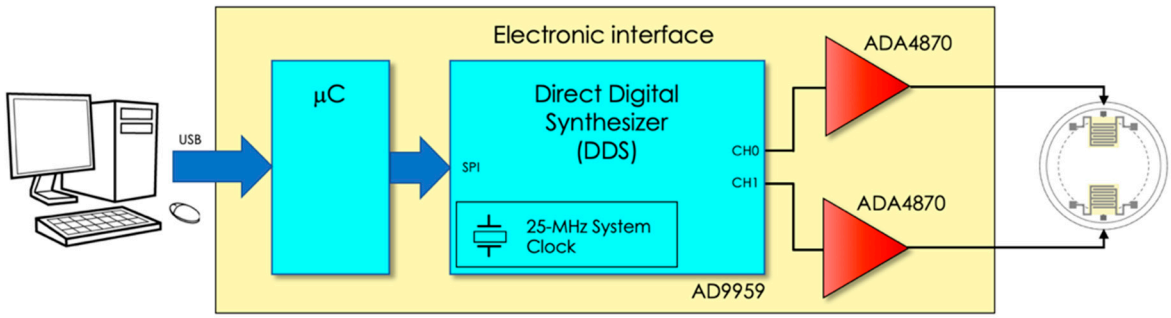

Figure 5. Block diagram of the tailored electronic interface used to drive the actuators.

4.2. Alignment of Cells

Preliminary tests have been carried out to verify the capability of the device to generate acoustic waves that lead to alignment of a cellular suspension. Cells to be aligned were detached from the culture dish, dispersed in PBS as single cells, stained with the live dye Neutral Red, and put in the chamber of the device. Figure 6 shows the experimental setup with the device placed under the optical microscope and the tailored electronic interface used to drive the piezoelectric actuators.

Initially, different concentrations of cells were tested in order to identify the amount required to appreciate the alignment in the volume of 500 µL, starting from 2×10^5 cells/mL and reaching 4×10^6 cells/mL. From these experiments, 2×10^6 cells/mL was identified as the optimal concentration for the formation of distinct lines of single cells, and therefore this amount was used for all the following experiments.

Since the survival of L6 rat myoblasts despite acoustic wave exposition was critical, this cell line was used to verify that the actuation was not hampering cell viability. The experiment was set up by exposing different samples with the same cell concentrations to FPWs for different lengths of time. Cell viability was then measured by trypan blue cell exclusion (Table 1). Since cell viability remained high even at long times, a 5-min actuation period was chosen for all the following experiments.

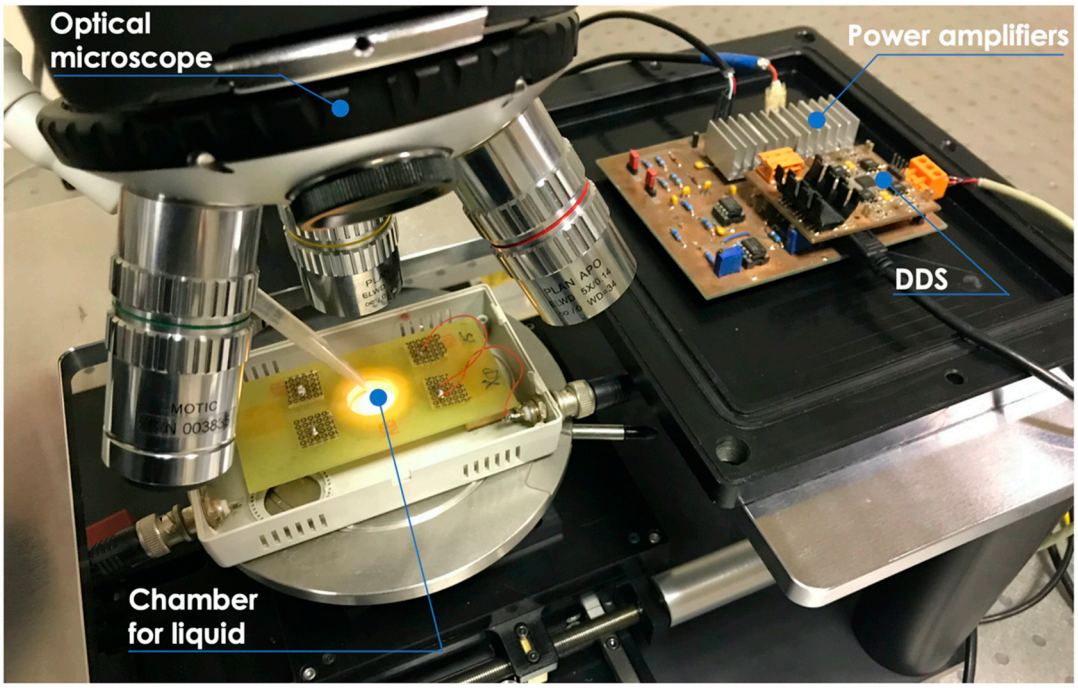

Figure 6. Experimental setup with the device placed under the optical microscope and the tailored electronic interface used to drive the piezoelectric actuators.

Table 1. Cell viability as a function of the actuation time of the device.

Actuation Time (min)	Cell Viability (%)
2	100
4	98
5	100
7	98

Different wavelengths were tested to verify the effects on the alignment of human fibroblasts (HFF) by exciting a single actuator with a sinusoidal signal applied to A and B (C was floating). To demonstrate the alignment of cells induced by the acoustic waves, HFF dispersed in PBS were used, since their viability is unaffected by the acoustic field.

The distance d between the different pressure nodes in the fluid, in which the cells are expected to be confined, corresponds to half the wavelength of the acoustic waves, resulting $d = \lambda/2 = v/2f_e$, where $v = 1500$ m/s is the expected propagation velocity of the acoustic waves into PBS, and f_e is the excitation frequency. Figure 7a,b show the results obtained with $f_{e1} = 6.7$ MHz and $f_{e2} = 8.0$ MHz, for which distances $d_1 = v/2f_{e1} = 112$ µm and $d_2 = v/2f_{e2} = 93.8$ µm are expected, respectively.

As it can be observed, an increase of the excitation frequency, i.e., decrease of the wavelength, corresponds to a decrease in the distance between lines. The mean distances between the cell alignments $d_{1,\text{mean}} = 121$ µm and $d_{2,\text{mean}} = 103$ µm, which are in good agreement with predictions, have been estimated from the gray-scale intensity plots derived from the insets. Similar results have been obtained by exciting a single actuator with a sinusoidal signal applied to A and B (shorted) and C with frequencies of 6.0 and 7.2 MHz (not shown).

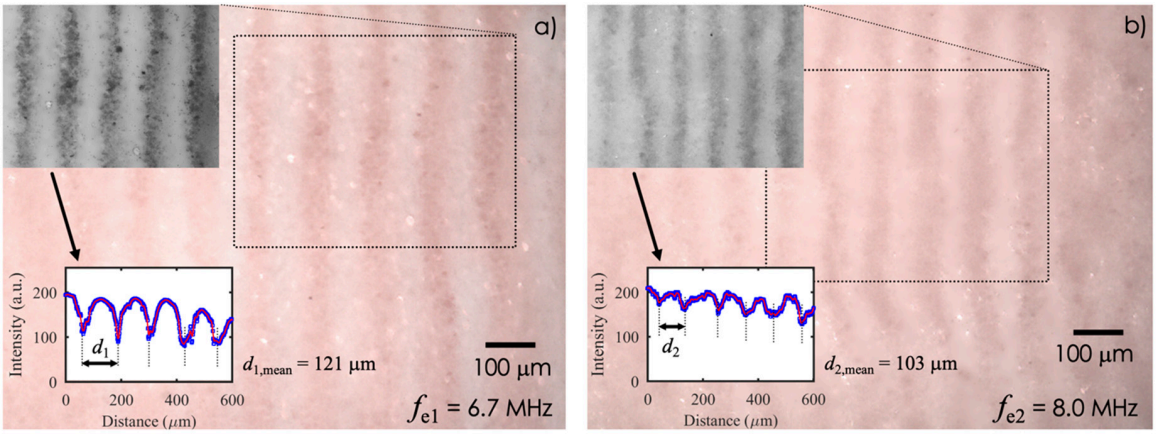

Figure 7. Effects of different wavelengths of acoustic waves on a human foreskin fibroblast (HFF) cell suspension. Cell accumulation in lines caused by the acoustic waves generated by exciting a single IDT at $f_{e1} = 6.7$ MHz (**a**) and $f_{e2} = 8.0$ MHz (**b**), respectively. The mean distances $d_{1,\text{mean}} = 121$ µm and $d_{2,\text{mean}} = 103$ µm have been estimated from the gray-scale intensity plots derived from the insets.

4.3. Entrapment of Cells in a Matrix

Switching off the actuator lets the cells scatter in the fluid, thereby losing the alignment. Hence, to maintain the cell alignment and separation, actuated cells have been entrapped in a 3D matrix.

To allow for wave propagation, a low-viscosity fluid capable of going through a sol–gel transition in a short time was needed, in which the polymerization had to start after the alignment. During the time needed for the sol–gel transition of the culture medium, i.e., five min in our experiments, the cell viability could be affected, given the impossibility of the cells, during this time, to make contact through the integrins with proteins of the cell matrix, a mechanism that has already been showed to regulate cell viability [29]. Relying on previous experience in the angiogenesis field, a fibrin gel, obtained by adding thrombin to a liquid fibrinogen solution, was used, rather than other biomaterials,

such as inert substrates mixed or linked to extracellular matrix molecules [8,30]. Besides, the survival of fibroblasts [31,32], fibroblasts/myoblasts [33], and HUVECs [34,35] in the fibrin gel has already been widely demonstrated. Cells were subsequently resuspended in a 10 mg/mL fibrinogen solution maintained at 4 °C, and thrombin 0.4 U was added just before transferring the cell suspension into the chamber. After five minutes, the fibrin clot was formed and aligned cells were entrapped in the matrix. For a long-term culture, the clots containing the cells were transferred to a cell culture dish, covered with cell culture medium, and observed in the following days. A 6.7 MHz excitation frequency was chosen for the following experiments.

The first experiments were done using rat myoblasts that, although totally alive after the actuation process, did not survive the following 24 hour culture, thereby suggesting that the stiffness of the fibrin matrix may not represent the correct environment for myoblast survival [36].

The next set of experiments was therefore performed with HFF. These cells entrapped in the fibrin clot maintained the aligned geometry for several days, as evidenced in Figure 8a–c, respectively. Of note, the magnification box in Figure 8a shows that each line is composed of single cells. Starting from 48 h, cells showed cytoplasmic protrusions, reflecting cell health, that became more complex over time, as shown in Figure 8d by a histological section of the clot and by the higher magnification box.

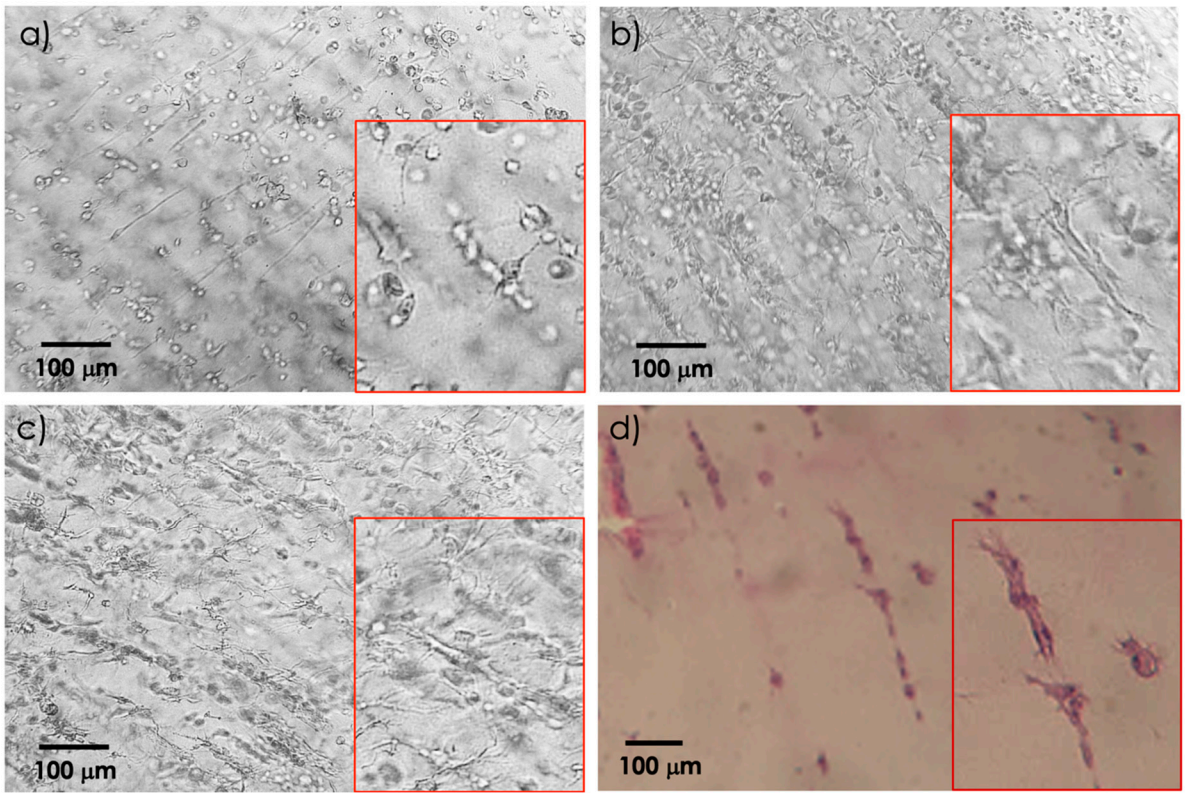

Figure 8. Aligned HFF in fibrin clot maintained in culture for 24 (**a**), 48 (**b**), and 72 h (**c**) with higher magnification boxes. Histological section of (hematoxylin and eosin)-stained cells at 72 h (**d**) with a higher magnification box.

4.4. Entrapment of Endothelial Cells in the Fibrin Clot

Angiogenesis assays are normally based on the capacity of endothelial cells to invade gels of different origins, mainly collagen or fibrin, and to form capillary-like structures [37]. Since the alignment could represent a preliminary step for the formation of a capillary, human endothelial cells were challenged in the device to verify the hypothesis that the process can promote it. Indeed, aligned HUVECs tend to form structures that become more complex during time. At 96 h

these structures still comprise several cells, as shown by microscope observations and nuclear DAPI staining in Figure 9a,b, respectively.

Next, the clot containing these structures was fixed, embedded in paraffin, and sliced, and the various sections underwent an immunochemical reaction with antibodies recognizing the CD31 endothelial antigen. In these conditions, HUVECs maintain the aligned organization that comprises a hole, as shown in Figure 9c.

To confirm that the alignment was based on a mechanical process, rather than a biological interaction, HUVECs were mixed with MSCs before the actuation. As those cells had similar sizes, their distribution along the pressure nodes was not clustered by cell type, as shown in Figure 9d. The presence of MSCs does not alter the cellular alignment, but the release of trophic factors characteristics of this type of cell [26,38] inhibits the formation of the hole, and promotes the formation of several cytoplasmic protrusions of HUVECs that are still recognized by their CD31 expression.

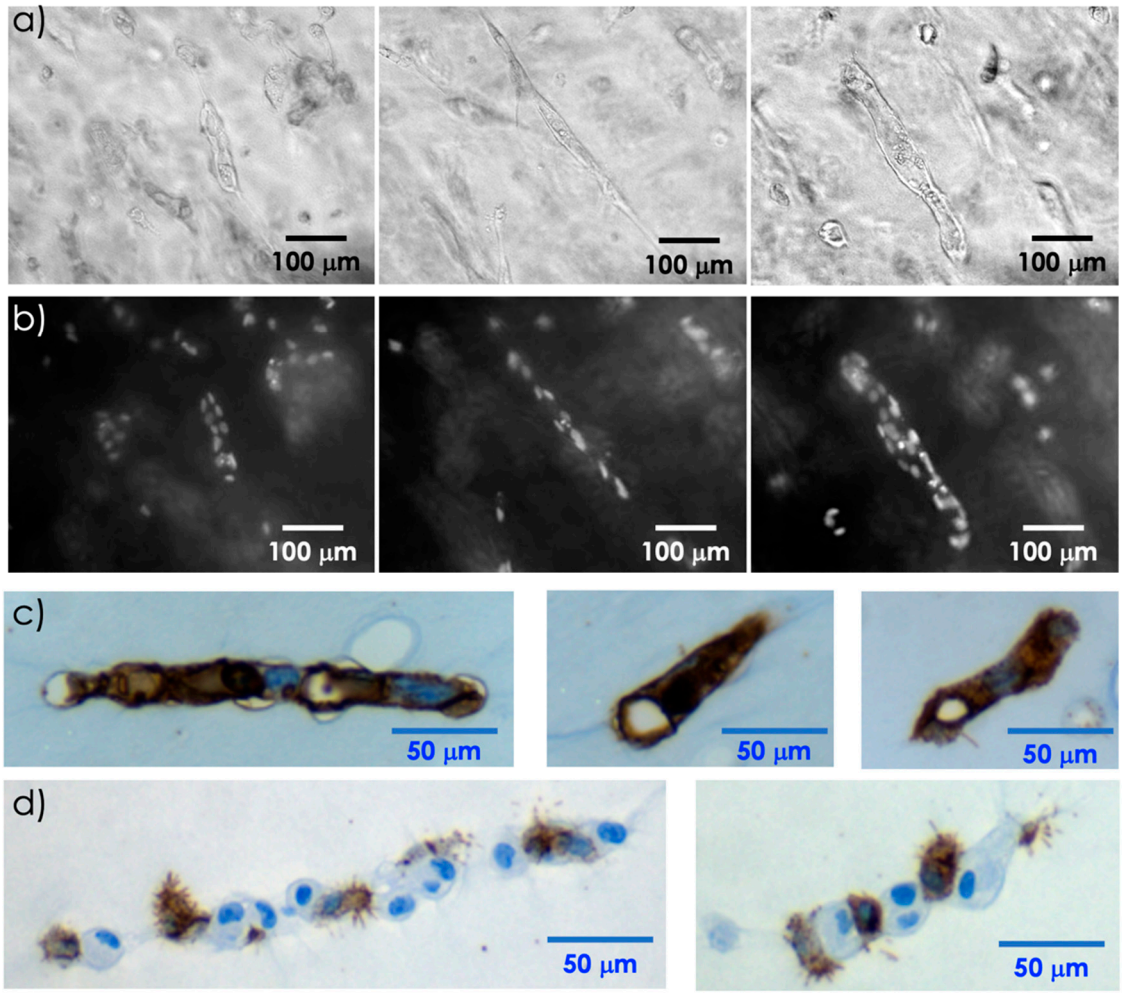

Figure 9. Aligned endothelial cells in fibrin clot at 96 h (**a**). DAPI staining showing cellular nuclei (**b**). CD31 (clone PECAM-1) staining of clot-entrapped human umbilical vein endothelial cells (HUVECs) (**c**). CD31 staining of clot-entrapped HUVECs and hMSCs (**d**).

5. Conclusions

The use of PZT actuators to generate acoustic waves in non-piezoelectric substrates has been proposed to steer and confine cells dispersed in liquid. A test device with two screen-printed PZT actuators used to generate acoustic waves on alumina substrate has been fabricated. The proposed device has the advantage of exploiting an inexpensive substrate which does not need to be piezoelectric, thereby allowing to use of high-temperature reinforced glasses which have the property of being

transparent. A tailored electronic circuit has been developed to generate the excitation signals for the actuators. Experimental results demonstrate that, by exciting a single actuator at its resonant frequencies, FPW modes are generated in the substrate. Accumulation of cells dispersed in liquid on lines can be obtained by selecting the proper excitation frequency. These results confirm the capability of the proposed PZT actuators to generate acoustic waves for applications in microfluidic devices as controlled positioning of cells dispersed in liquid.

From a biological point of view, devices similar to the one proposed are required to obtain ordered structures for tissue engineering purposes. Indeed, alignment of cells is a key step in several biological processes. For example, the basic unit of a muscle, i.e., the fiber, is formed by the fusion of several myocytes whose aligned actin and myosin molecules will produce effective muscle contraction [39]. Moreover, in engineered tissues, the presence of blood vessels that allow the distribution of nutrients or the cellular waste removal is an essential requirement. Therefore, the effective realization of an engineered tissue cannot be disjointed from an adequate architecture that, as shown, can be obtained using acoustic waves.

Author Contributions: Design and development of the device, M.F., M.D., M.B., and V.F.; experimental activity, M.B., M.D., M.S., S.C., and M.C.; analysis of experimental data, M.F., P.L.P., and P.D.; writing—original draft preparation, M.F. and P.D.; drawings, M.F.; writing—review and editing, M.F., M.B., V.F., M.S., and S.C.; funding acquisition, M.F, V.F., and P.D. All authors have read and agreed to the published version of the manuscript.

Funding: This research was funded by the project "MIcrosystems MeRging ACoustics and fLuidics to build human engineered tissuE (MIRACLE)" funded by University of Brescia in the context of "Health and Wealth 2015" athenaeum grant and partially supported by Fondazione Cariplo (grant number 2014-0822).

Conflicts of Interest: The authors declare no conflict of interest.

References

1. Guilak, F.; Butler, D.L.; Goldstein, S.A.; Baaijens, F.P. Biomechanics and mechanobiology in functional tissue engineering. *J. Biomech.* **2014**, *47*, 1933–1940. [CrossRef] [PubMed]
2. Bajaj, P.; Schweller, R.M.; Khademhosseini, A.; West, J.L.; Bashir, R. 3D biofabrication strategies for tissue engineering and regenerative medicine. *Annu. Rev. Biomed. Eng.* **2014**, *16*, 247–276. [CrossRef] [PubMed]
3. O'Brein, F.J. Biomaterials & scaffolds for tissue engineering. *Mater. Today* **2011**, *14*, 88–95.
4. Ratcliffe, A.; Niklason, L.E. Bioreactors and bioprocessing for tissue engineering. *Ann. N. Y. Acad. Sci.* **2002**, *961*, 210–215. [CrossRef] [PubMed]
5. Neumann, T.; Nicholson, B.S.; Sanders, J.E. Tissue engineering of perfused microvessels. *Microvasc. Res.* **2003**, *66*, 59–67. [CrossRef]
6. Murphy, S.V.; Atala, A. 3D bioprinting of tissues and organs. *Nat. Biotechnol.* **2014**, *32*, 773–785. [CrossRef]
7. The, R.; Yamaguchi, S.; Ueno, A.; Akiyama, Y.; Morishima, K.; Yamaguchi, S.; Ueno, A.; Akiyama, Y. Piezoelectric inkjet-based one cell per one droplet automatic printing by image processing. In Proceedings of the 2013 IEEE/RSJ International Conference on Intelligent Robots and Systems, Tokyo, Japan, 3–7 November 2013; pp. 502–507.
8. Naseer, S.M.; Manbachi, A.; Samandari, M.; Walch, P.D.K.; Gao, Y.; Zhang, Y.S.; Davoudi, F.; Wang, W.; Abrinia, K.; Cooper, J.M.; et al. Surface acoustic waves induced micropatterning of cells in gelatin methacryloyl (GelMA) hydrogels. *Biofabrication* **2017**, *9*, 015020. [CrossRef]
9. Song, K.; Wang, Z.; Liu, R.; Chen, G.; Liu, L. Microfabrication-Based Three-Dimensional (3-D) Extracellular Matrix Microenvironments for Cancer and Other Diseases. *Int. J. Mol. Sci.* **2018**, *19*, 935. [CrossRef]
10. Perry, J.L.; Kandlikar, S.G. Review of fabrication of nanochannels for single phase liquid flow. *Microfluid. Nanofluidics* **2006**, *2*, 185–193. [CrossRef]
11. Raimondi, M.; Moretti, M.; Cioffi, M.; Giordano, C.; Boschetti, F.; Laganà, K.; Pietrabissa, R. The effect of hydrodynamic shear on 3D engineered chondrocyte systems subject to direct perfusion. *Biorheol.* **2006**, *43*, 215–222.
12. Luo, J.K.; Fu, Y.Q.; Milne, W.I. Acoustic Wave Based Microfluidics and Lab-on-a-Chip. In *Modeling and Measurement Methods for Acoustic Waves and for Acoustic Microdevices*; IntechOpen: London, UK, 2013; pp. 515–556. [CrossRef]

13. Bouyer, C.; Chen, P.; Güven, S.; Demirtaş, T.T.; Nieland, T.J.F.; Padilla, F.; Demirci, U. A Bio-Acoustic Levitational (BAL) Assembly Method for Engineering of Multilayered, 3D Brain-Like Constructs, Using Human Embryonic Stem Cell Derived Neuro-Progenitors. *Adv. Mater.* **2016**, *28*, 161–167. [CrossRef] [PubMed]
14. Chen, Y.; Ding, X.; Lin, S.-C.S.; Yang, S.; Huang, P.-H.; Nama, N.; Zhao, Y.; Nawaz, A.A.; Guo, F.; Wang, W.; et al. Tunable Nanowire Patterning Using Standing Surface Acoustic Waves. *ACS Nano* **2013**, *7*, 3306–3314. [CrossRef] [PubMed]
15. Demori, M.; Baù, M.; Ferrari, M.; Ferrari, V. Interrogation Techniques and Interface Circuits for Coil-Coupled Passive Sensors. *Micromachines* **2018**, *9*, 449. [CrossRef] [PubMed]
16. Li, S.; Glynne-Jones, P.; Andriotis, O.G.; Ching, K.Y.; Jonnalagadda, U.S.; Oreffo, R.; Hill, M.; Tare, R.S. Application of an acoustofluidic perfusion bioreactor for cartilage tissue engineering. *Lab Chip* **2014**, *14*, 4475–4485. [CrossRef]
17. Guo, F.; Li, P.; French, J.B.; Mao, Z.; Zhao, H.; Li, S.; Nama, N.; Fick, J.R.; Benkovic, S.J.; Huang, T.J. Controlling cell–cell interactions using surface acoustic waves. *Proc. Natl. Acad. Sci. USA* **2015**, *112*, 43–48. [CrossRef]
18. Shilton, R.; Tan, M.K.; Yeo, L.Y.; Friend, J. Particle concentration and mixing in microdrops driven by focused surface acoustic waves. *J. Appl. Phys.* **2008**, *104*, 14910. [CrossRef]
19. Ding, X.; Lin, S.-C.S.; Kiraly, B.; Yue, H.; Li, S.; Chiang, I.-K.; Shi, J.; Benkovic, S.J.; Huang, T.J. On-chip manipulation of single microparticles, cells, and organisms using surface acoustic waves. *Proc. Natl. Acad. Sci. USA* **2012**, *109*, 11105–11109. [CrossRef]
20. Orloff, N.D.; Dennis, J.R.; Cecchini, M.; Schonbrun, E.; Rocas, E.; Wang, Y.; Novotný, D.; Simmonds, R.W.; Moreland, J.; Takeuchi, I.; et al. Manipulating particle trajectories with phase-control in surface acoustic wave microfluidics. *Biomicrofluidics* **2011**, *5*, 044107. [CrossRef]
21. Ai, Y.; Sanders, C.K.; Marrone, B.L. Separation of Escherichia coli Bacteria from Peripheral Blood Mononuclear Cells Using Standing Surface Acoustic Waves. *Anal. Chem.* **2013**, *85*, 9126–9134. [CrossRef]
22. Guo, F.; Mao, Z.; Chen, Y.; Xie, Z.; Lata, J.P.; Li, P.; Ren, L.; Liu, J.; Yang, J.; Dao, M.; et al. Three-dimensional manipulation of single cells using surface acoustic waves. *Proc. Natl. Acad. Sci. USA* **2016**, *113*, 1522–1527. [CrossRef]
23. Baù, M.; Ferrari, M.; Tonoli, E.; Ferrari, V. Sensors and energy harvesters based on piezoelectric thick films. *Procedia Eng.* **2011**, *25*, 737–744. [CrossRef]
24. De Luca, A.; Verardi, R.; Neva, A.; Benzoni, P.; Crescini, E.; Xia, E.; Almici, C.; Calza, S.; Dell'Era, P. Comparative Analysis of Mesenchymal Stromal Cells Biological Properties. *ISRN Stem Cells* **2013**, *2013*, 1–9. [CrossRef]
25. Ferrari, M.; Ferrari, V.; Marioli, D. Interface circuit for multiple-harmonic analysis on quartz resonator sensors to investigate on liquid solution microdroplets. *Sens. Actuators B Chem.* **2010**, *146*, 489–494. [CrossRef]
26. Arnau, A.; García, J.V.; Jiménez, Y.; Ferrari, V.; Ferrari, M. Improved electronic interfaces for AT-cut quartz crystal microbalance sensors under variable damping and parallel capacitance conditions. *Rev. Sci. Instrum.* **2008**, *79*, 75110. [CrossRef]
27. Demori, M.; Baù, M.; Ferrari, M.; Ferrari, V. Particle Manipulation by Means of Piezoelectric Actuators for Microfluidic Applications. *Lect. Notes Electr. Eng.* **2017**, *457*, 223–228. [CrossRef]
28. Demori, M.; Baù, M.; Dalola, S.; Ferrari, M.; Ferrari, V. Piezoelectric Actuators for In-Liquid Particle Manipulation in Microfluidic Applications. *Proceeding* **2017**, *1*, 392. [CrossRef]
29. Schwartz, M.; Assoian, R.K. Integrins and cell proliferation: Regulation of cyclin-dependent kinases via cytoplasmic signaling pathways. *J. Cell Sci.* **2001**, *114*, 2553–2560.
30. Sanzari, I.; Humphrey, E.J.; Dinelli, F.; Terracciano, C.M.; Prodromakis, T. Effect of patterned polyacrylamide hydrogel on morphology and orientation of cultured NRVMs. *Sci. Rep.* **2018**, *8*, 11991. [CrossRef]
31. Balestrini, J.L.; Billiar, K.L. Equibiaxial cyclic stretch stimulates fibroblasts to rapidly remodel fibrin. *J. Biomech.* **2006**, *39*, 2983–2990. [CrossRef]
32. Paye, M.; Nusgens, B.; Lapière, C. Factor XIII of Blood Coagulation Modulates Collagen Biosynthesis by Fibroblasts in vitro. *Pathophysiol. Haemost. Thromb.* **1989**, *19*, 274–283. [CrossRef]
33. Li, M.; Dickinson, C.E.; Finkelstein, E.B.; Neville, C.; Sundback, C.A. The Role of Fibroblasts in Self-Assembled Skeletal Muscle. *Tissue Eng. Part A* **2011**, *17*, 2641–2650. [CrossRef] [PubMed]

34. Nakatsu, M.; Sainson, R.C.; Aoto, J.N.; Taylor, K.L.; Aitkenhead, M.; Pérez-Del-Pulgar, S.; Carpenter, P.M.; Hughes, C.C. Angiogenic sprouting and capillary lumen formation modeled by human umbilical vein endothelial cells (HUVEC) in fibrin gels: The role of fibroblasts and Angiopoietin-1☆. *Microvasc. Res.* **2003**, *66*, 102–112. [CrossRef]
35. Nakatsu, M.; Hughes, C.C. Chapter 4 An Optimized Three-Dimensional In Vitro Model for the Analysis of Angiogenesis. *Methods Enzymol.* **2008**, *443*, 65–82. [CrossRef] [PubMed]
36. Gérard, C.; Forest, M.A.; Beauregard, G.; Skuk, D.; Tremblay, J.P. Fibrin Gel Improves the Survival of Transplanted Myoblasts. *Cell Transplant.* **2012**, *21*, 127–138. [CrossRef]
37. Taraboletti, G.; Giavazzi, R. Modelling approaches for angiogenesis. *Eur. J. Cancer* **2004**, *40*, 881–889. [CrossRef]
38. Hofer, H.R.; Tuan, R.S. Secreted trophic factors of mesenchymal stem cells support neurovascular and musculoskeletal therapies. *Stem Cell Res. Ther.* **2016**, *7*, 131. [CrossRef]
39. Lieber, R.L. Skeletal muscle adaptability. I: Review of basic properties. *Dev. Med. Child Neurol.* **1986**, *28*, 390–397. [CrossRef]